Top-Illuminated $In_{0.52}Al_{0.48}As$-Based Avalanche Photodiode With Dual Charge Layers for High-Speed and Low Dark Current Performances

Yi-Han Chen, Jhih-Min Wun, Song-Lin Wu, Rui-Lin Chao, Jack Jia-Sheng Huang, Yu-Heng Jan, H.-S. Chen, C.-J. Ni, Hsiang-Szu Chang, Emin Chou, and Jin-Wei Shi, *Senior Member, IEEE*

***Abstract*—A novel type of top-illuminated, etch-mesa $In_{0.52}Al_{0.48}As$-based avalanche photodiode (APD) with high-speed (>25 Gb/s), low dark current performance has been demonstrated. The 25G APD device is composed of n-side down design with the $In_{0.52}Al_{0.48}As$ multiplication (M) layer buried at the bottom to avoid the issues of surface breakdown and complex guard ring structure. In addition, we demonstrate that the new structure with two charge layers and triple mesas can effectively confine the electric-field within the center of M-layer and minimize the edge breakdown around the periphery of mesa. In contrast to the costly flip-chip bonding package with backside illumination, our demonstrated device is based on a simple top-illuminated structure that includes a large active diameter of 30 μm for easy optical alignment, a reasonable punch-through responsivity (0.7 A/W at 1.31 μm wavelength), and a good 3-dB optical-to-electrical (O-E) bandwidth (22.5 GHz) under low gain operations ($M_G = \sim 3$). Furthermore, it can sustain the 3-dB bandwidth of 15 GHz over a wide range of launched optical power (-17 to $+4.6$ dBm) under a moderate gain ($M_G = \sim 5$) operation at 1.31 μm wavelength. High-sensitivity (-16 dBm) for error-free 28 Gb/s operation can also be achieved at 1.55 μm wavelength.**

***Index Terms*—Avalanche photodiode, 100 Gbit/sec Ethernet.**

I. Introduction

THE relentless growth of global internet traffic is now driven by a new wave of traffic demand fueled by the latest applications such as mobile internet systems, cloud computing, and social networks. Among those applications, data centers have shown most explosive growth in recent years. Long-reach (LR4) and extended-reach (ER4) ethernet communications have gained popularity due to their capabilities to transmit signals over the distance of 10 km to 40 km between datacenter buildings [1]. Recently, the specification of ER-4 for 40 km at data rate of 100 Gb/s has been established (100GBASE-ER4) [1].

In 100 Gb/s ER-4 ethernet networks, 25 Gb/s emitters and photodetectors are key active components. The 25 G electro-absorption modulated lasers (EMLs) at 1.3 μm wavelength serve as the key light source in the ER-4 system [2]–[4]. One way to achieve good eye margin after 40 km transmission over fiber is to increase the optical output power ($> +3$ dBm) at the emitter end. On the other hand, increasing sensitivity at the receiving end is also an effective way to improve the overall transmission performance. Compared with p-i-n (PIN) photodiode receiver, APD can provide better sensitivity performance. For example, 1.55 μm APD showed sensitivity enhancement of about 8 dB over PIN at 10 Gb/s operation [5]. Hence, 25 Gb/s high-sensitivity APD has become a key component for 40 km photodetection over fiber in 100 Gbit/sec ER-4 system [6]–[8].

Among the reported material systems for the applications of high-speed APD [9], the $In_{0.52}Al_{0.48}As$-based multiplication (M-) layer has attracted significant attention during the development of 10 Gb/s and 25 Gb/s APD [9] due to its large gain-bandwidth product with reasonably low dark current characteristics at 1.3-1.5 μm wavelengths. Furthermore, the $In_{0.52}Al_{0.48}As$-based M-layer buried at the bottom epi-layer can eliminate the complicated guard-ring structures and avoid the problem of edge/surface breakdowns, compared to the InP-based M-layer at the topmost epi-layer [10]. The $In_{0.52}Al_{0.48}As$-based APD incorporates a small p-type mesa or Zn-diffusion region on top of the device for electric-field (E-field) confinement and >10 Gbit/sec operations [11], [12].

In order to further reduce the avalanche delay time in the M-layer for 25 Gbit/sec application, a thickness reduction in the $In_{0.52}Al_{0.48}As$ M-layer to less than 100 nm is necessary [9]. However, the maximum E-field in such a thin M-layer would reach around 900 kV/cm for high-sensitivity operation, thereby increasing the probability of edge breakdown at the periphery of mesa. To overcome such problem, an inverted $In_{0.52}Al_{0.48}As$-based (N-side up) APD has been demonstrated [6], [13]. Since

Manuscript received May 18, 2017; revised July 4, 2017; accepted July 21, 2017. Date of publication July 25, 2017; date of current version August 10, 2017. This work was supported in part by the Ministry of Science and Technology in Taiwan under Grant 105-2622-E-008-014-CC2 and in part by the Asian Office of Aerospace Research and Development under Grant FA2386-17-1-0033. *(Corresponding author: Jin-Wei Shi.)*

Y.-H. Chen, J.-M. Wun, S.-L. Wu, and J.-W. Shi are with the Department of Electrical Engineering, National Central University, Taoyuan 320, Taiwan (e-mail: willy111333@yahoo.com.tw; p3984011@hotmail.com; qazwsx830719@gmail.com; jwshi@ee.ncu.edu.tw).

R.-L. Chao is with the Department of Photonics, National Chiao-Tung University, Hsinchu 300, Taiwan, and also with the Department of Electrical Engineering, National Central University, Taoyuan 320, Taiwan (e-mail: obscurotation.eo03g@g2.nctu.edu.tw).

J. J.-S. Huang and Y.-H. Jan are with the Source Photonics, West Hills, CA 91304 USA, and also with the Source Photonics, Science-Based Industrial Park, Hsinchu 300, Taiwan (e-mail: jack.huang@sourcephotonics.com; yuheng.jan@sourcephotonics.com).

H.-S. Chen, C.-J. Ni, H.-S. Chang, and E. Chou are with the Source Photonics, Science-Based Industrial Park, Hsinchu 300, Taiwan (e-mail: hs.chen@sourcephotonics.com; cj.ni@sourcephotonics.com; hsiangszu.chang@sourcephotonics.com; emin.chou@sourcephotonics.com).

Color versions of one or more of the figures in this paper are available online at http://ieeexplore.ieee.org.

Digital Object Identifier 10.1109/JSTQE.2017.2731938

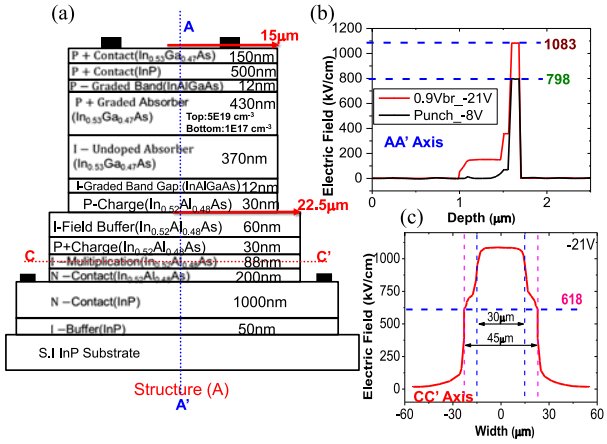

Fig. 1. (a) Conceptual cross-sectional view of the demonstrated structure A. The simulated E-field distributions in (b) vertical (A-A') and (c) horizontal directions (C-C').

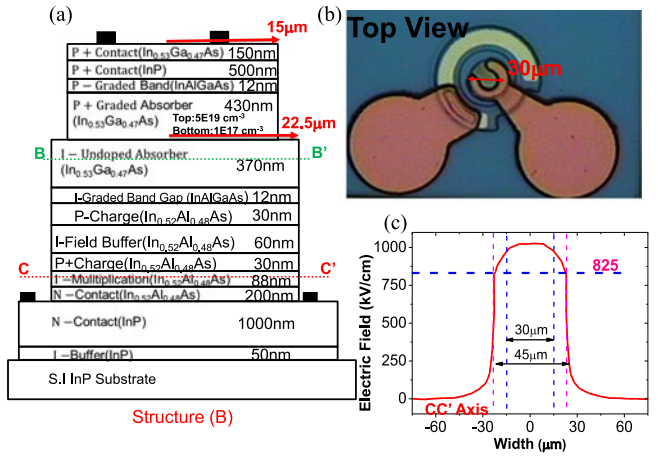

Fig. 2. (a) Conceptual cross-sectional view of the demonstrated structure B. (b) Photo of top-view of the fabricated devices. (c) The simulated E-field distribution in horizontal direction (C-C').

the $In_{0.52}Al_{0.48}As$ is placed near the top surface of such structure, the E-field at the M-layer is strongly influenced by the topmost n-type mesa. The inverted APD structure imposes design constraint in the charge and passivation layers due to the concerns of surface breakdown. In addition, the large active mesa with $In_{0.53}Ga_{0.47}As$ absorption layer at the bottom of device is also an issue for the optical alignment during the chip assembly process [14].

In this paper, we propose a novel N-side down APD with the $In_{0.52}Al_{0.48}As$-based M-layer buried at the bottom side of device. Compared with the traditional N-side down $In_{0.52}Al_{0.48}As$-based APDs [11], [12], our new device structure incorporates one additional charge layer above M-layer. By etching a mesa structure through the extra charge layer, the E-field can be strongly confined within the center of M-layer. It thus can consequently minimize the edge breakdown around the periphery of mesa and reduce the dark current. Furthermore, our demonstrated device is based on a simple top-illuminated structure that includes a large active diameter of 30 μm (with an optical window of 20 μm) for easy alignment, a reasonable punch-through responsivity (0.7 A/W at 1.31 μm wavelength), and a good 3-dB O-E bandwidth (22.5 GHz) under low gain operations ($M_G = \sim 3$). Furthermore, it can sustain the 3-dB bandwidth of 15 GHz over a wide range of launched optical power (-17 to $+4.6$ dBm) under a moderate gain ($M_G = \sim 5$) operation. High-sensitivity (-16 dBm) for error-free 28 Gbit/sec operation at the 1.55 μm wavelength can also be achieved.

II. Design of Device Structure and Fabrication

Figs. 1to 3 show the conceptual cross-sectional views of three demonstrated device structures in this work and their simulated E-field in vertical and horizontal directions. The simulation is conducted through the use of commercial software (Silvaco).[1] For simplicity, the cross-sectional views are not drawn in scale. As shown, all these three devices (A to C) have the same

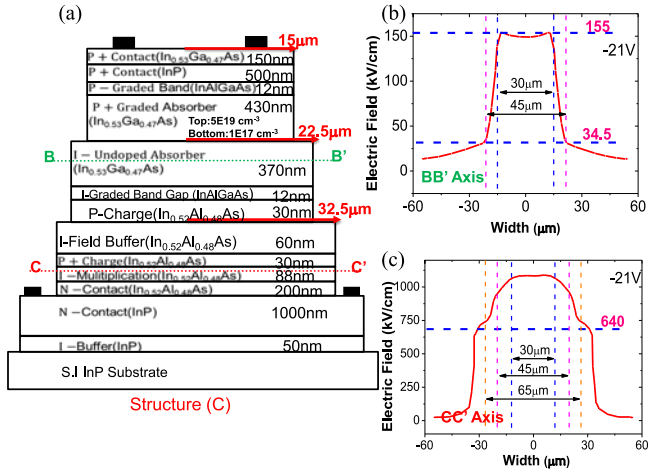

Fig. 3. (a) Conceptual cross-sectional view of the demonstrated structure C. The simulated E-field distribution in horizontal directions of (b) absorption layer (B-B') and (c) Multiplication layer (C-C').

epi-layer structure, which is grown by molecular-beam epitaxy (MBE) chamber[2] . From top to down, it is composed of the p^+-$In_{0.53}Ga_{0.47}As$ contact layer, p^+-InP window layer, p-type partially depleted $In_{0.53}Ga_{0.47}As$ absorber, two p-type $In_{0.52}Al_{0.48}As$ charge layers, one intrinsic $In_{0.52}Al_{0.48}As$ field buffer layer, one intrinsic $In_{0.52}Al_{0.48}As$ multiplication (M-) layer, and N^+ $In_{0.52}Al_{0.48}As$ /InP contact layers. Here, the partially depleted p-type absorber, which has a graded doping profile (top: 5×10^{19} to bottom 1×10^{17} cm^{-3}) is used to shorten the hole transit time, accelerate the electron diffusion process, and increase the high-power performance of our APD [15], [16]. Besides, two 12 nm graded bandgap layers (GBL) are inserted between the interfaces of p-type $In_{0.53}Ga_{0.47}As$/p-type InP window layers and depleted $In_{0.53}Ga_{0.47}As$/p-type $In_{0.52}Al_{0.48}As$ charge layers. Our GBL is mainly composed of

[1]Silvaco, Inc., 4701 Patrick Henry Drive, Bldg. 2, Santa Clara, CA 95054.

[2]Intelligent Epitaxy Technology, Inc, 1250 E Collins Blvd, Richardson, TX 75081.

four $In_{0.52-x}Al_xGa_yAs_{0.48-y}$ based bulk layers with a fixed layer thickness as 3 nm and four different bandgap wavelengths at 1, 1.2, 1.4, and 1.6 μm, respectively. Such design can minimize the probability of hole trapping in the interface of hetero-structures with bandgap discontinuity, which is an issue for APD operated at the high-gain and high-power regimes [17]. High-power performance is an important characteristic for the modern APD based receiver under burst-mode operation [6], which needs to tolerate the significant variation in the launched optical power and sustain the high-speed performance.

Here, the total thickness of $In_{0.53}Ga_{0.47}As$ absorber is 0.8 μm and the ratio of depleted versus p-doped region is around 0.86. According to our E-field simulation results shown in Fig. 1, such ratio would become 1.5 at around the optimized bias (-20 V) for high-sensitivity operation. This number (1.5) is chosen to balance the RC delay and internal carrier transit/avalanche-delay time under low gain operation ($M_G < 5$), which is based on our proposed bandwidth calculation model of APD [18]. The extracted RC- and transit time limited bandwidths of real fabricated device will be discussed latter. In order to shorten the avalanche delay time and meet the required high gain-bandwidth product of demonstrated device for the application of >25 Gbit/sec operation with high sensitivity, a thin M-layer (around 90 nm) is chosen in our device structure [9]. Although such thin M-layer may accompany with a significant tunneling current, the measured dark current of a well-fabricated APD with our novel E-field confinement structure is low and in the range of ~ 300 nA under 0.9 V_{br} bias, which will be discussed in detail latter. The shot noise induced by such amount of dark current should not be an issue for high-sensitivity >25 Gbit/sec operation of our device.

Compared with the traditional N-side down $In_{0.52}Al_{0.48}As$ based APD [11], [12], there is one extra charge layer and mesa structure, which are used to further reduce the E-field around the periphery of multiplication (M-) layer and minimize the probability of edge breakdown. As shown in Fig. 1(a), there is a triple mesa structure with different diameters in our device. The first mesa with a 30 μm diameter, is etched through the upper charge layer and stop at the 60 nm $In_{0.52}Al_{0.48}As$ buffer layer. Underneath the first mesa is the second mesa with a 45 μm diameter, which includes the lower charge layer and M-layer inside. The additional charge layer in the upper mesa is expected to effectively confine the strong E-field at the bottom M-layer within the range of 30 μm diameter. Fig. 1(b) and (c) shows the simulated E-field distributions in vertical and horizontal directions of our device at around optimized bias (-21 V) for high sensitivity operation, which will be discussed latter. As shown in Fig. 1(c), we can clearly see that the horizontal E-field in the M-layer within the range of 30 μm diameter is as high as 1000 kV/cm, and it can be greatly reduced to around 618 kV/cm at the edge of second mesa. Fig. 2 shows structure B with a mesa of 30 μm for the field confinement of M-layer. Compared to structure A in Fig. 1, the mesa etching depth of structure B is shallower. The etching only involved the p-type contact, p-type window layers, p-type absorber, and stopped at depleted $In_{0.53}Ga_{0.47}As$ absorption layer. This type of structure for field confinement of M-layer has been widely accepted in the 10 Gb/s $In_{0.52}Al_{0.48}As$ APD [12].

Fig. 2(c) shows the simulated horizontal E-field of the M-layer for structure B. Clearly, the additional mesa etch through the charge layer in our proposed novel device structure, as shown in Fig. 1, can have a stronger E-field confinement and smaller E-field in the periphery of M-layer (618 vs. 825 kV/cm).

The lower peripheral E-field could help reduce the edge breakdown. Besides, a careful design of sheet charge doping density in these two charge layers is important to prevent the $In_{0.52}Al_{0.48}As$ field buffer layer from reaching its critical E-field (around 550 kV/cm [19]).

Fig. 1 (b) shows the simulated E-field distribution in the vertical direction. We can clearly see that by properly adjusting the doping density in those two charge layers, the E-field in the buffer layer is around 300 kV/cm under -21 V bias. In addition, the corresponding E-field in the depleted $In_{0.53}Ga_{0.47}As$ absorption layer is at 150 kV/cm, which is around its critical field (150 kV/cm) [20] that may induce breakdown in the absorber layer and increase leakage current in the etched sidewall. A further adjustment in charge layer doping density is necessary to improve the device performance. In order to further reduce the dark current from the $In_{0.53}Ga_{0.47}As$ absorber, structure C has been fabricated, as shown in Fig. 3(a). Compared to structure A, there is one more extra mesa between the p-type and depleted $In_{0.53}Ga_{0.47}As$ absorption layers in order to attain E-field confinement in the absorption region. Fig. 3(b) and (c) shows the simulated E-field in the horizontal directions of depleted absorber and M-layer, respectively. By using such additional mesa structure, the peripheral E-field in the absorption region can be greatly reduced from 150 to 70 kV/cm. Nevertheless, compared with structure A, this mesa doesn't benefit the E-field confinement at the bottommost M-layer. As shown in Fig. 3(c), the simulated E-field in the periphery of M-layer is around 640 kV/cm, which is slightly larger than that of structure A (640 vs. 618 kV/cm) as shown in Fig. 1(c).

We adopted the $CH_4/H_2/Ar$ dry etching technique that exhibited a slow etching rate for the $In_{0.52}Al_{0.48}As$ material in order to precisely control the depth of mesa etch. After the mesa etch and p- and n-metal contacts, a thick (~ 5 μm) benzocyclobutene (BCB) film was used in the passivation process to reduce the dark current and to minimize the parasitic capacitance. An anti-reflection (AR) coating at 1.31 μm wavelength was deposited on the surface of our device to enhance its responsivity performance. Fig. 2(b) shows the top-view of our fabricated device with 30 and 20 μm diameters of active mesa and optical window, respectively. A co-planar stripe (CPS) was integrated with our device for on-wafer high-speed measurement. The layout of our CPS was suitable for traditional wire bonding assembly of the top-illuminated PDs or APDs, bringing cost advantage compared to the flip-chip package that was used in some 25G bottom-illuminated APDs [6], [7], [13].

III. Measurement Results

Fig. 4 shows the measured dark current of structures A to C where the trace of each device structure is indicated. It

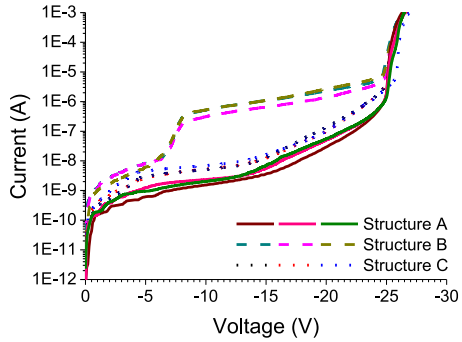

Fig. 4. The measured dark current of APD structures A, B and C.

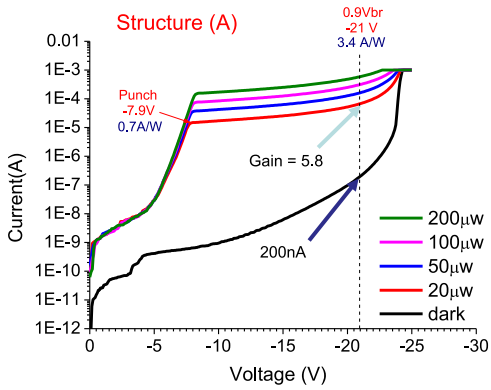

Fig. 5. The measured dark current and photocurrent of structure A versus bias voltages and under different optical pumping power at 1.31 μm wavelength.

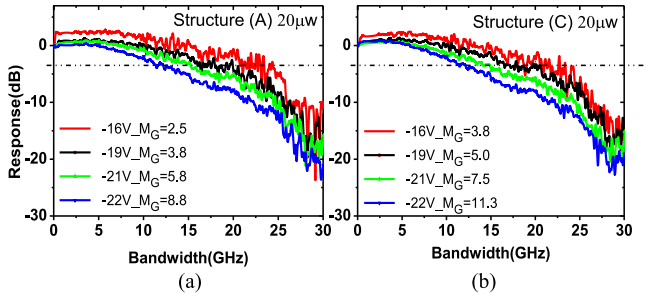

Fig. 6. The measured bias dependent O-E frequency responses of (a) structure A and (b) structure C under 20 μW optical pumping power at 1.31 μm wavelength.

can be clearly seen that both structures A and C have much lower leakage current than that of structure B as discussed in Figs. 1 to 3. In addition, the dark current of structure A was even slightly smaller than that of C, which has an extra mesa in $In_{0.53}Ga_{0.47}As$ absorber for E-field confinement as discussed in Fig. 3, implying that the leakage current from our absorption layer was not the major contributor in the total dark current of both devices. Furthermore, the smaller dark current in structure A might be attributed to the smaller E-field in the periphery of M-layer than that of structure C (640 vs. 618 kV/cm), as discussed in Figs. 1 and 3(c).

Fig. 5 shows the measured bias-dependent dark current and photocurrent of structure A subjected to different optical pumping power at the fixed optical wavelength of 1.31 μm, which is the desired central wavelength for ER-4 application [1]. The breakdown voltage (V_{br}) was at around 23.5 V and the corresponding dark current and operational gain at 0.9 V_{br} was around 200 nA and 5.8, respectively. During our measurement, we can assume a zero coupling loss from injected light onto our active device. This is because that the spot size of launched optical signal from lens fiber is much smaller than that of diameter of active optical window ($\sim$ 2 vs. 20 μm) and the anti-reflection (AR) coating on top of our device can provide a nearly zero reflection at 1.31 μm wavelength. With a 0.8 μm $In_{0.53}Ga_{0.47}As$ absorption layer thickness in our device, the theoretically maximum unit gain responsivity is around 0.58 A/W. The measured responsivity at punch-through point (-7.9 V) of our device (0.73 A/W) thus corresponds to 1.25 operation gain. When the bias voltage is below punch-through point, the E-field in the $In_{0.53}Ga_{0.47}As$ absorber is nearly zero and the measured small amount of photocurrent is mainly originated from the diffusion current. As can be seen, no matter how large the optical pumping power is, the small value (1 nA to 1 μA) of diffusion current of each trace is almost the same. It implies that most of the photo-generated carriers are recombined in the absorption region and can't be collected by the external circuits due the zero E-field inside absorber. Besides, the shift of punch-through point versus the optical pumping power is mainly due to the space charge screening (SCS) effect induced by the photo-generated carriers [21]. As can be seen, when the optical pumping power gradually increases, the Vpt shifts toward larger values due to that a higher bias voltage is necessary to compensate the space charge field induced by photo-generated carriers [21].

Compared with the reported dark current at $0.9\,V_{br}$ of bottom-illuminated APD for 25 Gbit/sec operation with a smaller mesa size (20 vs. 30 μm) [6], the obtained dark current here was even smaller (200 vs. $\sim$300 nA). Nevertheless, our device exhibited a lower responsivity performance than that of the reported data from 25 Gbit/sec bottom-illuminated APD (0.7 vs. 0.9 A/W at punch-through operations) [6]. This is because that the topmost contact metal in flip-chip bonding structure can serve as a mirror at the infrared wavelengths and result in a double pass of launched optical signal through the $In_{0.53}Ga_{0.47}As$ absorber. An enhancement in the responsivity performance can thus be obtained.

A lightwave-component-analyzer (LCA) system was utilized to characterize the dynamic performance of the device by measuring the frequency responses of the scattering (S) parameters. Such system was composed of a network analyzer (Anritsu 37397C), a well-calibrated electro-optics (E-O) modulator (MOD) operated at 1310 optical wavelengths, and a tunable semiconductor laser operated at 1310 nm as the light source for this system. The adopted E-O MOD was provided by Sumitomo (T.DEH1.5-40PD-ADC), which showed a 3-dB bandwidth of 30 GHz under 1310 nm optical pumping wavelength.

Fig. 6(a) and (b) shows the measured bias-dependent O-E frequency responses of structure A and C, respectively. The measured 3-dB bandwidths of the two structures were very close when being subject to the optical pumping power of 20 μW.

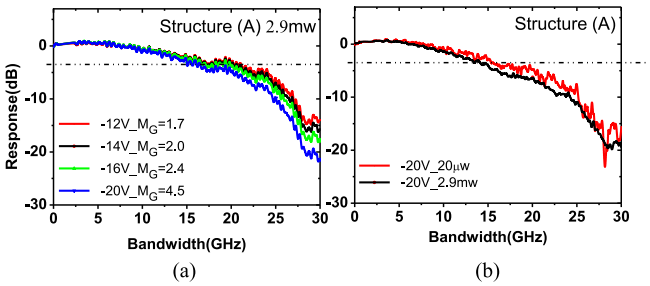

Fig. 7. (a) The measured bias-dependent O-E frequency responses of structure A under high optical pumping power (2.9 mW). (b) The measured O-E frequency responses of structure A under low (20 μW) and high (2.9 mW) optical pumping power at 1.31 μm wavelength. The bias voltage is fixed at -20 V ($M_G = 4.5$).

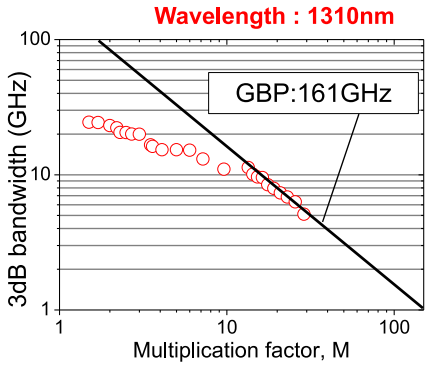

Fig. 8. The measured 3-dB O-E bandwidth versus multiplication gain of structure A at 1.31 μm wavelength. The fitted line shows the gain-bandwidth product.

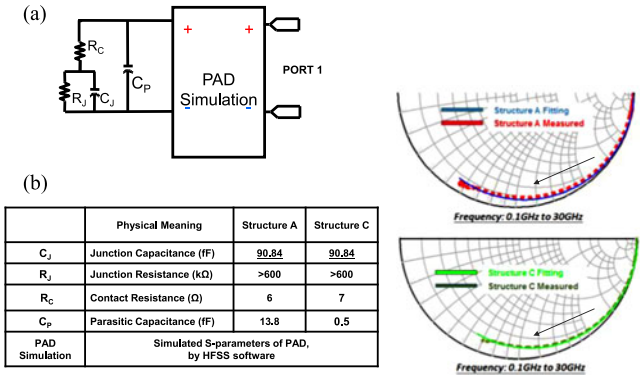

	Physical Meaning	Structure A	Structure C
C_J	Junction Capacitance (fF)	90.84	90.84
R_J	Junction Resistance (kΩ)	>600	>600
R_C	Contact Resistance (Ω)	6	7
C_P	Parasitic Capacitance (fF)	13.8	0.5
PAD Simulation	Simulated S-parameters of PAD, by HFSS software		

Fig. 9. Equivalent-circuit-model used for RC-bandwidth extraction. (b) Measured (dotted line) and fitted (solid line) S_{11} parameters from near DC to 30 GHz of structure A and C under a fixed bias (-20 V). The arrow indicates the increase in the sweeping frequency. The inserted table shows the extracted values of the components.

Under low optical pumping power and low operation gain ($M_G = \sim 3$ at -16 V) the measured 3-dB O-E bandwidths of structure A and C were both as high as around 22.5 GHz. When M_G reaches $6 \sim 7$ (at -21 V), the 3-dB bandwidths of the two devices degraded to around 15 GHz. As shown in Figs. 1 and 3, these two devices exhibited similar high-speed performance despite that structure C possessed a larger diameter of bottom active mesa than that of structure A (65 vs. 45 μm). The bandwidth results also suggested a close value of RC-limited bandwidth where the E-field was strongly confined by their topmost active mesa with the same diameter of 30 μm. The detail about their RC-limited bandwidth will be discussed later.

Maintaining highly linear performance of APD under strong launched optical signal (+4.6 dBm overloaded optical power) becomes an issue when the detected optical envelope with more advanced modulation format e.g., PAM-4 (pulse-amplitude-modulation with 4 amplitude levels) and for the application of burst-mode APD based receiver [6], [22]. Fig. 7(a) shows the measured bias-dependent O-E frequency responses of structure A under optical pumping power as high as 2.9 mW (+4.6 dBm). Fig. 7(b) shows the measured O-E frequency responses of the same device under a fixed reverse bias as -20 V with two different optical pumping power for comparison (20 μW and 2.9 mW). It was noted that the measured O-E bandwidth only degraded from 16 to 14 GHz over the wide range of launched optical power (-17 to +4.6 dBm) under moderate gain operation ($M_G = \sim 5$), which indicates the highly linear performance in our demonstrated APD structure.

Fig. 8 shows the multiplication gain versus the measured 3-dB O-E bandwidths of structure A. The achieved gain-bandwidth product (GBP) is around 161 GHz. We note that the GBP number is smaller than that of $In_{0.52}Al_{0.48}As$-based APDs (161 vs. $\sim$240 GHz) with similar M-layer thickness ($\sim$100 nm) [6], [23]. Such result can be attributed to that the undesired breakdown in the $In_{0.53}Ga_{0.47}As$ absorption layer under high gain operation ($M_G > 10$), as discussed in Fig. 1(b). To well-control the magnitude of E-field inside the $In_{0.53}Ga_{0.47}As$ absorber is a key issue, which determines the gain-bandwidth product performance of $In_{0.52}Al_{0.48}As$ based APD [24]. A larger value of GBP in our proposed device structure could thus be achieved by further adjusting the doping density in our dual charge layers to keep the E-field in $In_{0.53}Ga_{0.47}As$ absorption layer below its critical field ($\sim$ 150 kV/cm [20]) under V_{br} bias.

In order to investigate whether it is the carrier transit time or RC-bandwidth limitation that dominates the speed of our APDs, we performed the equivalent-circuit modeling technique to extract the RC-limited bandwidth of our device, as shown in Fig. 9(a). Here, the block of "Pad Simulation" represents the simulated scattering (S) parameters of CPS in our device, as shown in Fig. 2(b). The values used in fitting process are shown in the Table inserted into Fig. 9(b), which shows the measured and simulated frequency responses for the microwave reflection coefficient parameter (S_{11}) under a -20 V bias of structures A and B; see the Smith chart. Clearly, the simulated and measured results match very well, from 100 MHz to 30 GHz. Based on the established equivalent circuit model, we can thus extract the RC-limited frequency responses of structures A and C, which are shown as solid line traces in Fig. 10. As can be seen, the extracted RC-limited 3-dB bandwidth of structure A and C is very close and at 33 and 36 GHz, respectively. The similar RC-limited bandwidth of these two devices indicate that the junction capacitance (C_J) is determined by the size of topmost p-type mesa, which strongly confines the E-field in absorption and M-layers as discussed in Figs. 1 to 3.

According to the measured net O-E bandwidth (22.5 GHz) under low gain operation, the corresponding transit time limited

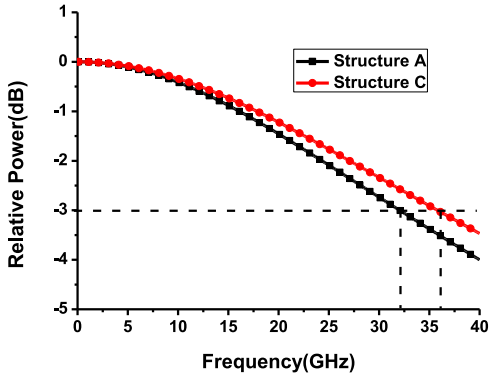

Fig. 10. The extracted RC-limited frequency responses of structure A and C.

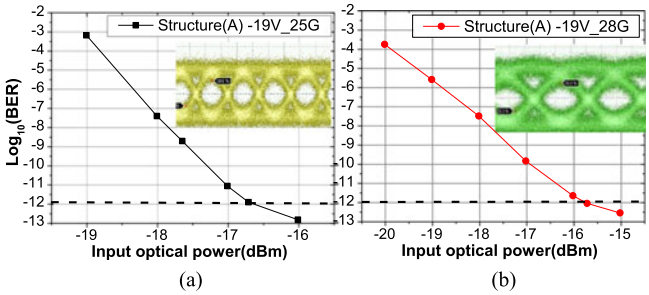

Fig. 11. The measured BER curves vs. received optical power at (a) 25 and (b) 28 Gbit/sec operations at 1.55 μm optical wavelength. The inset shows the measured error-free 25 and 28 Gbit/sec eye-patterns under -17.2 and -16 dBm, respectively.

bandwidth is around 31 GHz. This value is fairly close to our extracted RC-limited bandwidth, which indicates the validity of our bandwidth calculation model and design flow of optimized APD epi-layer structure [18].

Fig. 11 shows the measured 25 and 28 Gbit/sec bit-error-rate (BER) curves versus received optical power of structure A under 1.55 μm wavelength excitation. The inset shows the error-free eye-patterns with -17.2 and -16 dBm optical received power under 25 and 28 Gbit/sec operations, respectively. The optical pseudorandom binary sequence (PRBS) with $2^{15}-1$ pattern length was generated by use of a 1550 nm E-O modulator (Sumitomo: T.DEH1.5-40PD-ADC) under 3.5 V peak-to-peak radio-frequency (RF) voltage driving. The estimated extinction ratio is around 6 dB. Here, the optical wavelength at 1.55 μm instead of 1.3 μm was chosen is due to that the modulator we have on hand only can generate high-quality eye-patterns at 1.55 μm wavelength. During eye-pattern measurements, our PD was integrated with a broadband (100 kHz to 65 GHz) amplifier (Centellax, UA0L65VM) through a microwave probe and coaxial cable. The amplified O-E converted eye-patterns were then fed into the bit-error-rate (BER) tester or sampling scope to record their BER values and waveforms. The bias voltage applied to our APD was set at -19 V, which corresponded to operation gain of around 4 for the optimized sensitivity performance at 1.55 μm optical wavelength. It was shown that the error-free sensitivity of -17.2 (-16) dBm was achieved at 25 (28) Gbit/sec. The

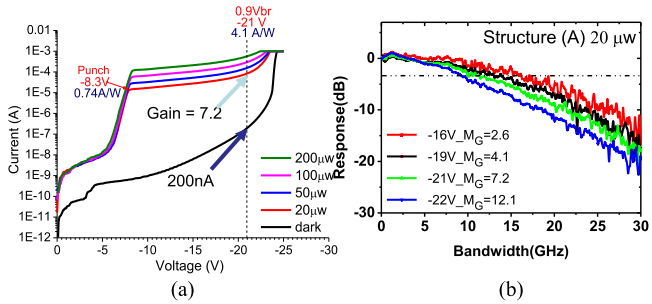

Fig. 12. (a) The measured dark current and photocurrent of structure A versus bias voltages and under different optical pumping power at 1.55 μm wavelength. (b) The measured bias dependent O-E frequency responses of structure A under 20 μW optical pumping power at 1.55 μm wavelength.

achieved sensitivity here may satisfy the specification for the application of 100 GbE-ER4-lite [25], which requires a receiver operated at 25 Gbit/sec and 1.31 μm optical wavelength with a -19 dBm sensitivity under a BER value of 5×10^{-5} instead of error-free.

A higher sensitivity was expected by integrating our APD chips with a 25 Gbit/sec trans-impedance amplifier (TIA) in the 100 Gbit/sec ROSA package. For most cases, the TIA amplifier usually can provide a better S/N ratio than that of RF broadband amplifier for amplifying the weak photocurrent signal. In addition, the sensitivity may be further enhanced by shifting the wavelength of our eye-pattern measurement system from 1.55 to 1.31 μm wavelength. Fig. 12(a) shows the measured bias-dependent dark current and photocurrent of structure A with the AR-coating at 1.55 μm wavelength and subjected to different optical pumping power at such wavelength. Compared with the measurement results of the same device structure but at 1.31 μm wavelength operation, as discussed in Fig. 5, the measured punch-through responsivity (~ 0.7 A/W) and operation gain are pretty close. Here, the unit gain at 1.55 μm wavelength is around 0.59 A/W, which is obtained through using the same definition as the case of 1.31 μm wavelength. This result indicates that the responsivity is not an issue in the quality of our measured eye-patterns across these two wavelengths (1.31 to 1.55 μm).

On the other hand, as shown in Fig. 12(b), the measured bias dependent O-E frequency responses at 1.55 μm shows a narrower 3-dB bandwidth (~ 13 vs. ~ 16 GHz) compared to the operation at 1.31 μm and under the same optical pumping power (20 μW) with the operation gain ($M_G = 6-7$ at -21 V bias). Such discrepancy in speed performance can be attributed to different absorption depths in our p-type absorption region [26] when the optical wavelength varies from 1.31 to 1.55 μm wavelength. It is a subject for future study. According to such dynamic measurement results, we can thus expect that the sensitivity performance of our device can be further improved under 1.31 μm wavelength operation due to the enhancement in speed performance.

IV. Conclusion

In conclusion, we have demonstrated a novel top-illuminated $In_{0.52}Al_{0.48}As$-based APD for $>$ 25 Gbit/sec operation at

1.31 μm wavelength without using costly flip-chip bonding package. By using dual charge layers with special mesa structure, the E-field can be strongly confined in the center of bottommost $In_{0.52}Al_{0.48}As$ based M-layer. Compared with reference device with different mesa etching depths for E-field confinement, our device can have a much lower dark current. By optimizing the depletion width in our partially p-doped $In_{0.53}Ga_{0.47}As$ absorber to balance the RC-delay and internal carrier transient time, our device that incorporates the active mesa of 30 μm show advantages including easy optical alignment, reasonable punch-through responsivity ($\sim 0.7\,A/W$), and high-speed performance with 3-dB bandwidth of ~ 22.5 GHz under low gain operation ($M_G = \sim 3$) at 1.31 μm optical wavelength. Furthermore, when the overload of optical power reaches +4.6 dBm, our device still can sustain >20 GHz 3-dB bandwidth. High-sensitivity of -16 dBm for error-free 28 Gbit/sec operation can be achieved at 1.55 μm optical wavelength, which can further be improved by integrating our device with a TIA in a ROSA module and shift the measurement wavelength to 1.31 μm wavelength.

REFERENCES

[1] 2009. [Online]. Available: http://www.ieee802.org/3/ba/

[2] T. Fujisawa *et al.*, "First 40-km SMF transmission for 100-Gbit/s ethernet system based on 25-Gbit/s 1.3-μm electroabsorption modulator integrated with a DFB laser module," in *Proc. 35th Eur. Conf. Optical Commun.*, Vienna, Austria, Sep. 2009, pp. 8.6.4.

[3] S. Kanazawa *et al.*, "Flip-chip interconnection lumped-electrode EADFB laser for 100-Gb/s/λ transmitter," *IEEE Photon. Technol. Lett.*, vol. 27, no. 16, pp. 1699–1701, Aug. 2015.

[4] T. Tatsumi, K. Tanaka, S. Sawada, H. Fujita, and T. Abe, "1.3 μm, 56-Gbit/s EML Module target to 400 GbE," in *Proc. Opt. Fiber Commun. Conf.*, Los Angeles, CA, USA, Mar. 2012, Paper OTh3F.4.

[5] 2006. [Online]. Available: http://www.ieee802.org/3/av/public/2006_11/3av_0611_lee_1.pdf

[6] M. Nada, T. Yoshimatsu, Y. Muramoto, H. Yokoyama, and H. Matsuzaki, "Design and performance of high-speed avalanche photodiodes for 100-Gb/s systems and beyond," *IEEE/OSA J. Lightw. Technol.*, vol. 33, no. 5, pp. 984–990, Mar. 2015.

[7] Albis Optoelectronics AG, Moosstrasse 2a, Rueschlikon, Switzerland. (Product: APD 16L on Submount), 2013.

[8] D. Pan *et al.*, "Cost-effective 25G APD TO-Can/ROSA for 100G applications," in *Proc. Opt. Fiber Commun.*, Los Angeles, CA, USA, Mar., 2017, Paper Th3B.3.

[9] J. C. Campbell *et al.*, "Recent advances in avalanche photodiodes," *IEEE J. Sel. Topics Quantum Electron.*, vol. 10, no. 4, pp. 777–787, July/Aug. 2004.

[10] M. A. Itzler, K. K. Loi, S. McCoy, N. Codd, and N. Komaba, "Manufacturable planar bulk-InP avalanche photodiodes for 10 Gb/s applications," in *Proc. Opt. Fiber Commun. Conf.*, San Diego, CA, USA, Feb. 1999, pp. 748–749.

[11] E. Ishimura *et al.*, "Degradation mode analysis on highly reliable guarding-Free Planar InAlAs avalanche photodiodes," *IEEE/OSA J. Lightw. Technol.*, vol. 25, no. 12, pp. 3686–3693, Dec. 2007.

[12] B. F. Levine *et al.*, "A new planar InGaAs-InAlAs avalanche photodiode," *IEEE Photon. Technol. Lett.*, vol. 18, no. 18, pp. 1898–1900, Sep. 2006.

[13] M. Nada, H. Yokoyama, Y. Muramoto, T. Ishibashi, and H. Matsuzaki, "50-Gbit/s vertical illumination avalanche photodiode for 400-Gbit/s ethernet systems," *Opt. Express*, vol. 22, no. 12, pp. 14681–14687, Jun. 2014.

[14] M. Nada, Y. Muramoto, H. Yokoyama, T. Ishibashi, and H. Matsuzaki, "Triple-mesa avalanche photodiode with inverted P-Down structure for reliability and stability," *IEEE/OSA J. Lightw. Technol.* vol. 32, no. 8, pp. 1543–1548, Apr., 2014.

[15] X. Li *et al.*, "High-saturation-current InP-InGaAs photodiode with partially depleted absorber," *IEEE Photon. Technol. Lett.*, vol. 15, no. 9, pp. 1276–1278, Sep. 2003.

[16] Y.-S. Wu *et al.*, "High performance evanescently edge coupled photodiodes with partially p-Doped photo-absorption layer at 1.55 μm wavelength," *IEEE Photon. Technol. Lett.*, vol. 17, no. 4, pp. 878–880, Apr., 2005.

[17] J. C. Campbell, W. S. Holden, G. J. Qua, and A. G. Dentai, "Frequency response of InP/InGaAsP/InGaAs avalanche photodiodes with separate absorption "Grading" and multiplication regions," *IEEE J. Quantum Electron.*, vol. QE-21, no. 11, pp. 1743–1746, Nov. 1985.

[18] J.-W. Shi and C.-W. Liu, "Design and analysis of separate-absorption-transport-charge-multiplication traveling-wave avalanche photodetectors," *IEEE/OSA J. Lightw. Technol.*, vol. 22, no. 6, pp. 1583–1590, Jun. 2004.

[19] M. A. Saleh *et al.*, "Impact-ionization and noise characteristics of thin III-V avalanche photodiodes," *IEEE Trans. Electron Devices*, vol. 48, no. 12, pp. 2722–2731, Dec. 2001.

[20] Y. L. Goh, J. S. Ng, C. H. Tan, W. K. Ng, and J. P. R. David, "Excess noise measurement in In0.53Ga0.47As," *IEEE Photon. Technol. Lett.*, vol. 17, no. 11, pp. 2412–2414, Nov. 2005.

[21] K. Kato, "Ultrawide-band/high-frequency photodetectors," *IEEE Trans. Microw. Theory Technol.*, vol. 47, no. 7, pp. 1265–1281, Jul. 1999.

[22] M. Nada *et al.*, "High-linearity avalanche photodiode for 40-km transmission with 28-Gbaud PAM-4," in *Proc. Opt. Fiber Commun. Conf.*, Los Angeles, CA, USA, Mar., 2015, Paper M3C.2.

[23] M. Lahrichi *et al.*, "240-GHz gain-bandwidth product back-side illuminated alinas avalanche photodiodes," *IEEE Photon. Technol. Lett.,* vol. 22, no. 18, pp. 1373–1375, Sep. 2010.

[24] N. Duan *et al.*, "Detrimental effect of impact ionization in the absorption region on the frequency response and excess noise performance of InGaAs-InAlAs SACM avalanche photodiodes," *IEEE J. Quantum Electron.*, vol. 41, no. 4, pp. 568–572, Apr., 2005.

[25] 2013. [Online]. Available: http://www.ieee802.org/3/bm/public/smfadhoc/meetings/apr16_13/cole_03_0413_smf.pdf

[26] J.-W. Shi, K.-L. Chi, C.-Y. Li, and J.-M. Wun, "Dynamic analysis of high-efficiency INP based photodiode for 40 Gbit/sec optical interconnect across a wide optical window (0.85 to 1.55 μm)," *IEEE/OSA J. Lightw. Technol.*, vol. 33, no. 4, pp. 921–927, Feb. 2015.

Yi-Han Chen was born in Kaohsiung, Taiwan, on December 10, 1992. He is currently working toward the Master's degree in the Department of Electrical Engineering, National Central University, Taoyuan, Taiwan. His current research interests include high-speed and high-sensitivity avalanche photodiode.

Jhih-Min Wun was born in Taoyuan, Taiwan on October 03, 1988. He is currently working toward the Ph.D. degree in the Department of Electrical Engineering, National Central University, Taoyuan, Taiwan. His current research interests include high-speed optoelectronic device measurement and sub-THz high-speed photodiode.

Song-Lin Wu was born in Taipei, Taiwan, on July 19, 1994. He is currently working toward the Master's degree in solid state physics from the Department of Electrical Engineering, National Central University, Taoyuan, Taiwan. His current research interests include high-speed and high-performance avalanche photodiode.

Rui-Lin Chao was born in Taipei, Taiwan on October, 27, 1991. He received the B.S. degree in Undergraduate Honors Program of Nano Science and Engineering, Chiao Tung University, Hsinchu, Taiwan, in 2014, and currently working toward the Ph.D. degree in the Department of Elecro-Optics, Chiao Tung University, under guidance from advisor Prof. J. Chen, and also under guidance of Co-advisor Prof. J.-W. Shi, National Central University, focusing on slow light high speed silicon-based modulator, high-speed photodetector and high-speed laser development and design.

Jack Jia-Sheng Huang received the B.S. degree in physics from National Taiwan University, Taipei, Taiwan, in 1992, and the M.S. and Ph.D. degrees in materials science from UCLA in 1996 and 1997, respectively. In 1997, he received Outstanding Ph.D. Award and Dissertation Year Fellowship Award from Henry Samueli School of Engineering, UCLA. He is currently a Sr. R&D Scientist/Manager at Source Photonics, working on Advanced Photonics Devices including 100G EML, 40G CWDM DFB, 10G DFB, and 10G FP lasers as well as 10G and 25G APD photodetectors. His R&D projects also involve device reliability physics and device characterization. He has more than 80 publications in international journals and conferences in the areas of optoelectronics and ICs. He holds 6 U.S. patents and 1 U.K. patent. From 2000 to 2015, he was a Wafer Fab R&D/Operations Manager in Emcore, working on device design/process/characterization, reliability, electrostatic discharge (ESD) and failure analysis of analog BH lasers and digital ridge lasers for cooled and uncooled applications. From 1997 to 2000, he was a Member of Technical Staff at Lucent Technologies, Bell Labs, Orlando, FL, USA, working on electromigration, stress migration, and failure analysis of 0.3, 0.25, 0.2, and 0.16 mm ASIC and FPGA devices using CMOS technology. During 1992–1993, he was a Research Assistant at the Institute of Atomic and Molecular Sciences, Academia Sinica, Taiwan, studying surface physics of gallium ion beam in ultrahigh vacuum.

Yu-Heng Jan was born in Taipei, Taiwan, on November 6, 1965. He received the Ph.D. degree in electrical and computer engineering from the University of California, Santa Barbara, CA, USA, in 1997. In 1997, he joined the Optical Division of MRV communication where he focused on the design and manufacturing of CWDM DFB lasers and systems. In 2007, he became COO and the General Manager of Taiwan Division of Source Photonics, where he managed Operations and RD activities. He served **a**s the Chief Device Officer at Source Photonics, where he focused on high speed devices for Data Center and PON applications.

H.-S. Chen received the Ph.D. degree from Graduate Institute of Photonics and Optoelectronics, Nation Taiwan University, Taipei, Taiwan, in 2006. Since June 2007, he has been a Postdoctoral Research Fellow with the Institute of Physics, Acadmia Sinica. From 2011 to 2013, he has been with the Institute of Photonics and Optoelectronics, Nation Taiwan University, as a Postdoctoral Fellow. His research interests include surface plasmon, near field optics, ultrafast laser, nanorod array LED, and optical sensors. In 2014, he joined the Source Photonics Inc., as a Manager of Advanced Process Development.

C.-J. Ni received the B.S. degree in chemical engineering from National Chung Cheng University, Chiayi, Taiwan, in 2006, and the M.S. and Ph.D. degrees in chemical engineering from National Cheng Kung University, Tainan, Taiwan, in 2008 and 2014, respectively. He is currently an R&D Engineer at Source Photonics Inc., a Division of Advanced Process Development.

Hsiang-Szu Chang received the M.S. and Ph.D. degrees from Solid-State Optics Laboratory, Department of Physics, National Central University, in 2002 and 2009, respectively. He is currently working at Source Photonics Inc., as a Sr. Engineer of Product Development, OE device.

Emin Chou received the B.S. degree in nuclear engineering from National Tsing Hua University, Hsinchu, Taiwan, in 1997, and the M.S. degree in MBE Laboratory, Department of Electronics Engineering from National Chiao Tung University, Taiwan, in 1999. He is currently working at Source Photonics Inc., as the Sr. Director of Product Development, Advanced OSA, and OE Devices.

Jin-Wei Shi (M'03–SM'12) was born in Kaohsiung, Taiwan, on January 22, 1976. In 2003, he joined the Department of Electrical Engineering, National Central University, Taoyuan, Taiwan, where he is a Professor since 2011. In 2011–2012 and 2016, he joined the ECE Department of UCSB as a Visiting Professor. His current research interests include ultrahigh speed/power photodetectors, electroabsorption modulator, THz photonic transmitter, and VCSELs. He has authored or coauthored more than 4 book chapters, 120 Journal papers, 180 conference papers, and hold 30 patents. He received 2010 Da-You Wu Memorial Award.